A K-band high PAE wide tuning range VCO Using triple-coupled LC tanks

Mahalingam, Nagarajan; Ma, Kaixue; Yeo, Kiat Seng; Lim, Wei Meng

2013

Mahalingam, N., Ma, K., Yeo, K. S., & Lim, W. M. (2013). A K-band High PAE Wide Tuning Range VCO Using Triple-Coupled LC Tanks. IEEE Transactions on Circuits and Systems II: Express Briefs, 60(11), 736-740.

https://hdl.handle.net/10356/100214

https://doi.org/10.1109/TCSII.2013.2281751

A *K*-band High PAE Wide Tuning Range VCO Using Triple-Coupled LC Tanks

Nagarajan Mahalingam, *Student Member*, *IEEE*, Kaixue Ma, *Senior Member, IEEE,*
Kiat Seng Yeo, *Senior Member, IEEE,* and Wei Meng Lim

***Abstract*— This paper presents a fully differential *K*-band voltage-controlled oscillator (VCO) using commercial 0.18µm SiGe BiCMOS process. By using triple-coupled LC tanks with strong coupling and varactor controlled capacitor bank, the proposed VCO achieves wide tuning range, low phase noise, high output RF power and high power added efficiency (PAE) simultaneously. The implemented VCO demonstrates an oscillation frequency range from 22.50 GHz to 26.23 GHz, frequency tuning range of 15.3%, phase noise of -107.7 dBc/Hz at 1 MHz offset, output power of -3.1 dBm, power added efficiency of 5.97% and a figure-of-merit (FOM) of -186.9 dBc/Hz with a DC power of 8.2 mW.**

***Index Terms*— 24 GHz, Coupled LC tanks, Frequency Tuning Range (FTR), K-band, Low Power, Phase Noise, SiGe, VCO.**

I. Introduction

RECENTLY, high data-rate communication systems with increased bandwidth requirements have drawn much attention. To realize wideband and high data rate systems with good performance, it is critical for VCO in the local oscillator to have a wide tuning range with low phase noise and high output power. However, the stringent constraint on low power consumption, severely limits the achievable phase noise, tuning range and especially the power added efficiency (PAE).

Transformer based VCOs with low power low phase noise are reported in [1] – [4] but these works have narrow tuning range and relatively lower output power. Improvement in tuning range is achieved in [5] with dual LC tanks at source and drain terminals but the VCO has a lower output power. High quality transmission line VCOs are reported in [6], [7], but these designs have narrow tuning range and higher phase noise respectively. Inductor based VCOs are reported in [8] - [10] but these designs have narrow tuning range and low output power. Although many VCOs addressed on different aspects like tuning range, power consumption, phase noise, etc., have been reported in literature, it still remains a challenge to design VCOs with optimized trade-off to simultaneously achieve a wide tuning range, low phase noise, high output power and good PAE (P_{out}/P_{DC}).

In this paper, we present a fully differential *K*- band Colpitts VCO extending the work in [11] to address the VCO operation based on the theoretical analysis. This design achieves a wide tuning range, low phase noise, high output power and good PAE simultaneously, by using the proposed triple-coupled LC tanks with varactor and capacitor banks. The strong coupling of LC tanks and proper choice of coupling coefficient increase not only the equivalent tank quality factor and VCO tuning range but also the delivered output power and PAE. The operation mechanism of the tank circuit is investigated theoretically using the equivalent circuit model and verified experimentally based on a commercial SiGe BiCMOS process.

This paper is organized as follows: In section II, analysis of triple-coupled LC tanks and the implementation of the proposed VCO is presented. Section III gives the measurement results and the conclusion is presented in Section IV.

Manuscript received April 23, 2013, revised July 9, 2013, accepted August 6, 2013. This work was supported by Exploit Technologies Private Limited, Singapore and Nanyang Technological University, Singapore.

N. Mahalingam, K. Ma and K. S. Yeo are currently with School of Electrical and Electronic Engineering, Nanyang Technological University, Singapore, 639798, email: nagarajan@ntu.edu.sg, kxma@ieee.org .

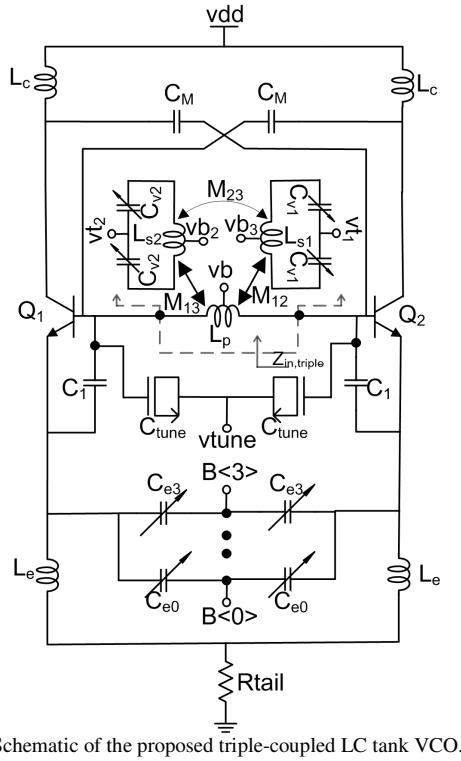

Fig. 1. Schematic of the proposed triple-coupled LC tank VCO.

II. Circuit Design and Analysis

The circuit schematic of the proposed Colpitts VCO is shown in Fig. 1. The negative resistance of the Colpitts oscillator is generated by the fixed capacitor C_1, transistor base-emitter parasitic capacitance C_π and coarse tuning varactors in the emitter ($C_{e0} – C_{e3}$). In the proposed VCO, the triple-coupled LC

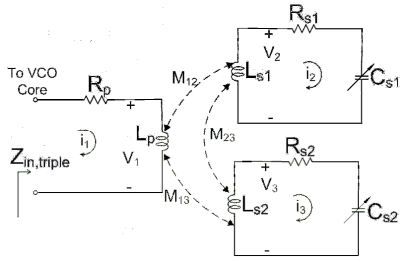

Fig. 2. Simplified circuit schematic of triple-coupled LC tanks.

tanks is formed by magnetically coupled coils L_p, L_{s1} and L_{s2} together with capacitor/varactor banks (C_{ei}, i=0~3, C_{v1}, C_{v2} and C_{tune}). The primary L_p is connected to the fine tuning varactors C_{tune} and base of transistors Q_1 and Q_2 while the secondary coils L_{s1} and L_{s2} are connected to MOS varactors C_{v1} and C_{v2} respectively. The VCO in Fig. 1 is completed by degeneration inductor L_e and tuned circuit at the collector formed by L_c and C_M. The degeneration inductor improves the VCO signal feedback [11], while the combination of L_c and C_M improves the negative resistance in the frequency band of interest reducing the power consumption to be discussed in part C of this section. All the MOS varactors in Fig. 1 are based on accumulation mode MOS varactors with minimum possible device length.

A. Analysis of triple-coupled LC tanks

The simplified circuit schematic of the triple-coupled coils is shown in Fig. 2. The self inductance of the primary and secondary coils of the triple-coupled LC tanks is given by L_p, L_{S1} and L_{S2} respectively; R_p represents the loss in the primary coil, C_{S1} and C_{S2} represent the total effective capacitances connected to the two secondary coils formed by capacitance of varactors C_{v1} and C_{v2} respectively; R_{S1} and R_{S2} represent the losses in secondary coils respectively. Based on circuit theory, the impedance matrix of the triple-coupled LC tanks is:

$$\begin{bmatrix} V_1 \\ V_2 \\ V_3 \end{bmatrix} = \begin{bmatrix} P & -j\omega M_{12} & -j\omega M_{13} \\ -j\omega M_{21} & S_1 & -j\omega M_{23} \\ -j\omega M_{31} & -j\omega M_{32} & S_2 \end{bmatrix} \begin{bmatrix} i_1 \\ i_2 \\ i_3 \end{bmatrix} \quad (1)$$

where, $P = R_p+j\omega L_p$, $S_1 = R_{s1}+j\omega L_{s1}+(j\omega C_{s1})^{-1}$, $S_2 = R_{s2}+j\omega L_{s2}+(j\omega C_{s2})^{-1}$. Considering $M_{ij}=M_{ji}$ due to symmetry, the input impedance of the triple-coupled LC tanks can be derived as given in (2) , where, the first term represents the primary impedance; the other terms represent the coupling between the primary and the two secondary coils; and $M_{ij} = K_{ij}\sqrt{L_i L_j}$. From (2), the input impedance of the triple-coupled LC tanks can be simplified as shown in (3) – (6) assuming $R_{s1} = R_{s2} = R_s$, $L_{s1} = L_{s2} = L_s$ and $C_{s1} = C_{s2} = C_s$. To gain more design insight, the input impedance of triple-coupled LC tanks can be further simplified neglecting higher order terms as

$$Z_{triple,simplified} = R_{triple,simplified} + j\omega L_{triple,simplified} \quad (7)$$

where,

$$R_{triple,simplified} = \left[R_p + \frac{R_s\left[M_1\left(L_{sc}^4 + L_{sc}^2\omega^2 M_{23}^2\right) + M_2\left(4\omega L_{sc}^3\right)\right]}{R_{dr}^2 + L_{dr}^2} \right] = [R_p + R_{eff}] \quad (8)$$

$$L_{triple,simplified} = \left[L_p + \frac{\frac{L_{sc}^2}{\omega}\left[\omega^2 M_{23}^2\left(L_{sc}M_1 + 2\omega M_2\right) - \left(L_{sc}^3 M_1 + 2\omega M_2 L_{sc}^2\right)\right]}{R_{dr}^2 + L_{dr}^2} \right] = [L_p + L_{eff}] \quad (9)$$

where, $M_1 = \omega^2(M_{12}^2+M_{13}^2)$, $M_2 = (\omega^2 M_{12}M_{13}M_{23})$ and $L_{sc} = (\omega L_s)-(\omega C_s)^{-1}$. The quality factor of the triple-coupled LC tanks when ω equals VCO operating frequency ω_0, can be derived as:

$$Q_{triple} = \frac{\omega_o\left(L_p + L_{eff}\right)}{R_p + R_{eff}} \quad (10)$$

B. Layout and validation of triple-coupled LC tanks

The layout of the triple-coupled LC tanks is shown in Fig. 3 and the simulated self inductance, quality factor and coupling coefficient based on EM simulation is shown in Fig 4. To validate the effect of the coupling coefficient on the quality factor of the triple-coupled LC tanks, Equation (10) is plotted as shown in Fig. 5. For the simulations, simulated parameters in Fig. 4(a) is used assuming equal coupling coefficients (k_{12}=k_{13}=k_{23}=k), R_p = 0.65 Ohm, R_s = 1 Ohm, L_p = L_s = 100 pH and C_s = 100 fF at 24 GHz. From Fig. 5, it can be observed that the quality factor can be enhanced by providing a stronger coupling between the coils of the triple-coupled LC tanks. The increase in tank's quality factor improves the energy transfer efficiency of the resonator and enhances the PAE and phase noise of the oscillator [12].

In triple-coupled LC tanks, the effect of quality factor of the secondary coils on Q_{triple} cannot be neglected. To validate the

$$Z_{in,triple} = P + \frac{\omega^2 M_{13}^2}{S_2} + \frac{\omega^2 M_{12}^2 S_2}{\omega^2 M_{23}^2 + S_1 S_2} + \frac{2j\omega M_{12}\cdot\omega^2 M_{13} M_{23}}{\omega^2 M_{23}^2 + S_1 S_2} - \frac{\omega^4 M_{13}^2 M_{23}^2}{S_2\left(\omega^2 M_{23}^2 + S_1 S_2\right)} \quad (2)$$

$$Z_{in,triple} = R_{triple} + j\omega L_{triple} = \left[R_p + \left(\frac{R_{eff,tri}}{R_{dr}^2 + L_{dr}^2} \right) \right] + j\omega \left[L_p + \left(\frac{\frac{L_{eff,tri}}{\omega}}{R_{dr}^2 + L_{dr}^2} \right) \right], where \quad (3)$$

$$R_{eff,tri} = R_s^5 M_1 + R_s^3\left[M_1\left(2L_{sc}^2 + \omega^2 M_{23}^2\right) + 2\omega M_2(3L_{sc} - 1)\right] + R_s\left[M_1\left(L_{sc}^4 + L_{sc}^2\omega^2 M_{23}^2\right) + M_2\left(4\omega L_{sc}^3\right)\right] \quad (4)$$

$$L_{eff,tri} = \left[-3R_s^5 L_{sc} M_1 + 2R_s^4\left(L_{sc}M_1 + \omega M_2\right) + R_s^2\left[M_1\left(L_{sc}\omega^2 M_{23}^2 - 2L_{sc}^3 \right)\right] + M_2\left(2\omega^3 M_{23}^2 \right)\right] + L_{sc}^2\left[\omega^2 M_{23}^2\left(L_{sc}M_1 + 2\omega M_2\right) - \left(L_{sc}^2\left(L_{sc}M_1 + 2\omega M_2\right)\right)\right] \quad (5)$$

$$R_{dr} = R_s^3 - 3R_s L_{sc}^2 + \omega^2 M_{23}^2 R_s \text{ and } L_{dr} = 3R_s^2 L_{sc} - L_{sc}^3 + \omega^2 M_{23}^2 L_{sc} \quad (6)$$

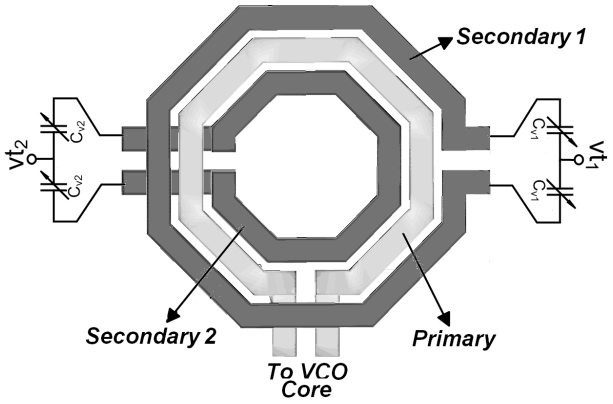

Fig. 3. Layout of triple-coupled LC tanks (Center-tap not shown).

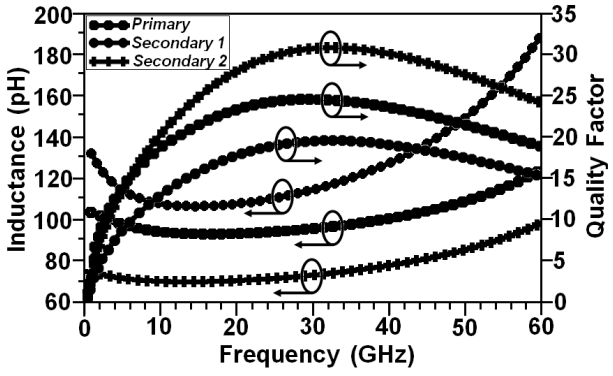

(a)

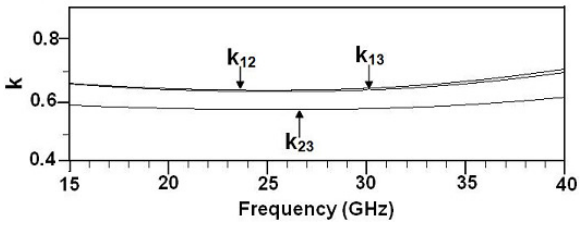

(b)

Fig. 4. Simulated parameters of triple-coupled coils (a) Inductance and quality factor, (b) coupling coefficient between coupled coils.

effect, secondary coil resistive loss (R_s) is varied and the resulting Q_{triple} and L_{triple} is plotted in Fig. 6. Simulated parameters in Fig. 4 are used by assuming a frequency of 24 GHz and a fixed secondary coil capacitance of 200 fF. It can be observed that, the increased resistive losses in the secondary coils degrade the quality factor of the coupled LC tanks and reduction of R_s is desired to maintain the overall quality factor of the triple-coupled LC tanks (Q_{triple}). Also from Fig. 6, it can

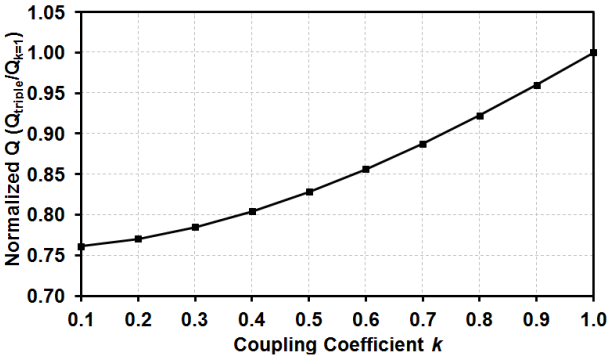

Fig. 5. Variation of Q_{triple} with coupling coefficient k.

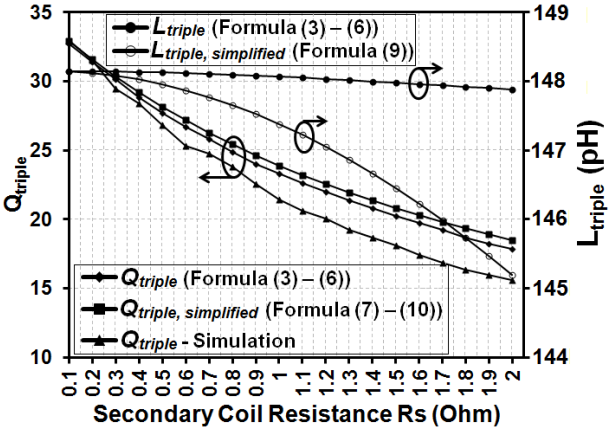

Fig. 6. Variation of Q_{triple} and L_{triple} with secondary coil resistance R_s.

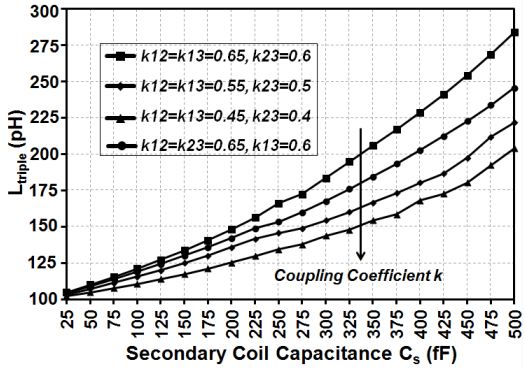

Fig. 7. Variation of L_{triple} with secondary coil capacitance C_s.

be seen that the variation in L_{triple} is quite small as R_s is increased.

To understand the effect of the coupling coefficient on the VCO frequency tuning range, the variation in L_{triple} is plotted in Fig. 7 for different coupling coefficients between the primary and two secondary coils against the secondary coil capacitance C_s. From Fig. 7, it can be observed that, the maximum variation in L_{triple} is achieved when strong coupling is present between the primary and the two secondary coils. From (9), intuitively, $L_{sc}{}^3 M_1$ term dominates the effective inductance and M_1 increases with strong coupling between the primary and secondary coils. Therefore, with strong coupling and digitally tuning the secondary coil capacitance C_s, the tuning range of the VCO can be maximized by tuning the VCO operating frequency using the large variation in L_{triple}.

The phase noise of the Colpitts oscillator is given by [13]

$$S_{\Delta out} = 2\frac{\left\langle \overline{|i_n|}^2 \right\rangle}{|V_{tank}|^2}\frac{1}{(C_1+C_\pi)^2\left(\frac{C_1+C_\pi}{C_{ei(i=0to3)}}+1\right)}\frac{1}{\Delta\omega^2} \qquad (11)$$

where, $S_{\Delta out}$ denotes the phase noise spectral density, $\left\langle \overline{|i_n|}^2 \right\rangle$ is the average input white noise power of the transistor, V_{tank} is the tank swing and $\Delta\omega$ is the offset from the carrier angular frequency. From (11), it can be seen that, the phase noise is influenced by the quality factor of tank circuit and effect on capacitor ratio formed by C_1, base emitter capacitance C_π and total capacitance connected to the emitter of transistors Q_1 and Q_2. To characterize the VCO phase noise performance due to capacitor and transistor mismatch, the proposed VCO was

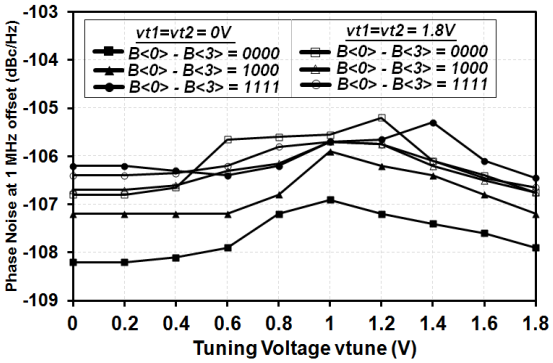

Fig. 8. Simulated phase noise using Monte-Carlo analysis.

simulated by using Monte-Carlo analysis. The analysis considers the process and mismatch models provided by the foundry including the self-heating in Hicum BJT models. With a total of 100 samples, the simulated VCO phase noise at 1 MHz offset over the entire frequency range and varying vtune is shown in Fig. 8. From the data it can be seen that the phase noise discrepancy of the VCO is within 3 dB over the entire VCO operating range. This change in the phase noise can be attributed to the change in the quality factor of the varactors used for digital coarse tuning in the VCO.

C. *Improvement of negative resistance*

Though Colpitts oscillator can achieve a lower phase noise, they consume high DC power to achieve the required negative resistance for reliable startup [12]. For the Colpitts oscillator, the negative resistance is given by

$$\mathrm{Re}\{Z_{in}\} = R_{neg} = -\frac{g_m}{\omega^2 C_{1T} C_{equi}} \qquad (12)$$

where, $C_{1T} = C_1 + C_\pi$ and C_{equi} is the equivalent capacitance

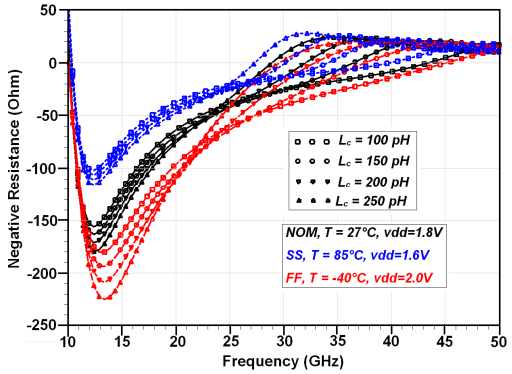

Fig. 9. PVT simulation of negative resistance for varying L_C without C_M.

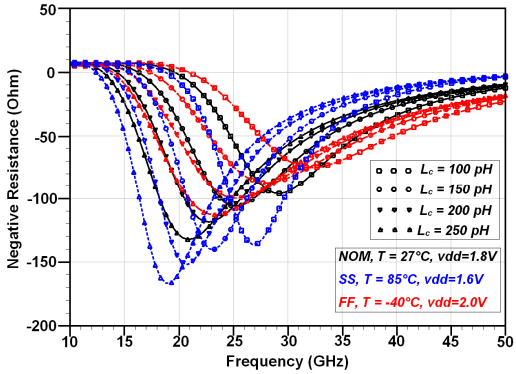

Fig. 10. PVT simulation of negative resistance for varying L_C with C_M.

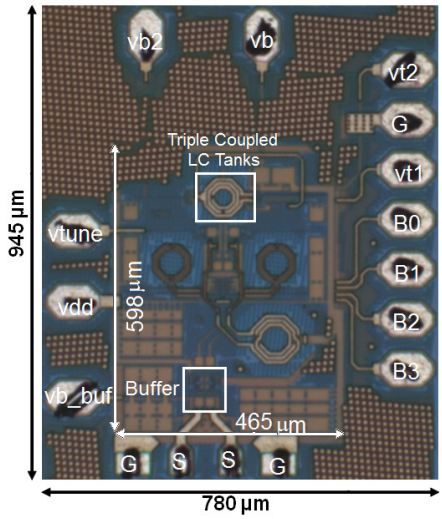

Fig. 11. VCO Die-microphotograph.

connected across the transistor emitter terminals. For low frequencies, the effect of transistor's collector-base capacitance C_{BC} is usually neglected and the negative resistance defined by Equation (12) is sufficient. For low power Colpitts VCO operating in *K*-band and above, the presence of C_{BC} makes negative resistance in (12) inadequate. This could pose a serious issue for VCO startup in the presence of PVT variations. To comprehend the effect of C_{BC} across the process corners, the negative resistance of the proposed VCO is simulated with different L_c values. From Fig. 9, it can be observed that, after 10 GHz, as L_c increases, the available negative resistance decreases and the usable range is reduced. In the proposed VCO, as shown in Fig 1, the capacitor C_M in combination with L_c improves the negative resistance in the frequency band of interest as shown in Fig. 10.

III. Experimental Results

The die-microphotograph of the proposed VCO implemented in Tower Jazz 0.18 µm SiGe BiCMOS process with f_T of 200 GHz is shown in Fig. 11. The VCO and buffer consume an area of 465 µm × 598 µm excluding the measurement pads. The triple-coupled coils are implemented with available top metal thickness of 2.81 µm and k is around 0.65 (upper limit is process dependent). With a dc supply voltage of 1.8 V, the VCO core consumes 8.2 mW and the buffer consumes 5.4 mW. The VCO

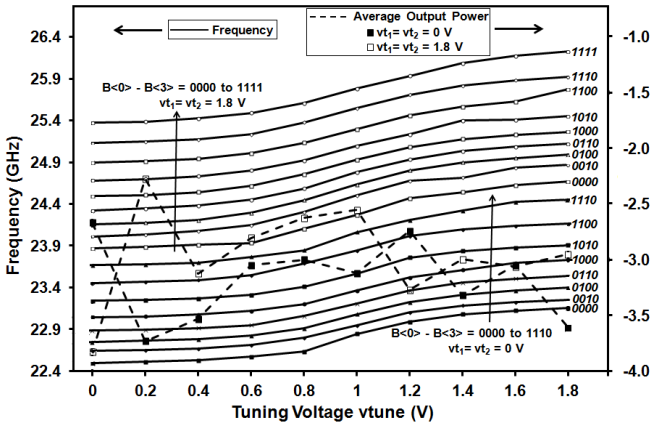

Fig. 12. Measured VCO tuning range and average output power.

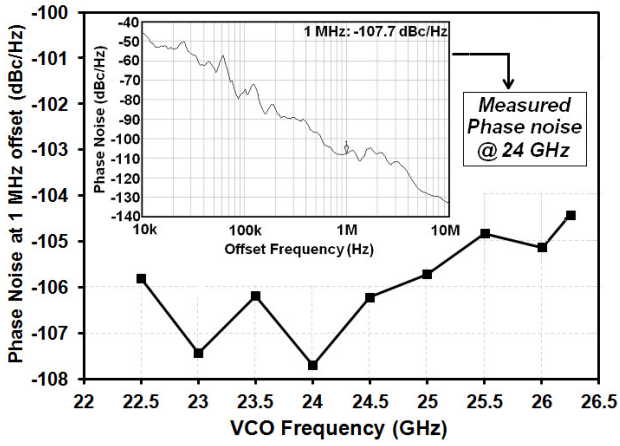

Fig. 13. Measured VCO phase noise.

is measured on-wafer varying the fine tuning voltage vtune and coarse tuning bits B<0> - B<3> by digitally controlling vt_1 and vt_2 to 0 V or 1.8 V. As shown in Fig. 12, the proposed VCO covers frequencies from 22.50 GHz to 26.23 GHz, a frequency tuning range of 15.309%. Excluding the simulated buffer loss of 3.2 dB, the VCO measures an average single-end output power of -3.1 dBm for varying vt_1 and vt_2 as shown in Fig. 12. The phase noise of the proposed VCO across the operational frequency is shown in Fig. 13. The VCO achieves a lowest phase noise of –107.7 dBc/Hz at 1 MHz and -132 dBc/Hz at 10 MHz offset from 24 GHz carrier as shown in Fig. 13. A comprehensive summary and comparison with VCOs in the same frequency range is shown in Table I. For a fair comparison, the SiGe VCO in Table I have a similar f_t as in this work. As can be observed from Table I, the proposed VCO achieves a wide tuning range with low K_{VCO}, low phase noise, high output power and high PAE simultaneously which are important for high performance low power application VCOs.

IV. Conclusion

In this work, a fully differential *K*-band VCO using the triple-coupled LC tanks is presented. The strong coupling of triple-coupled LC tanks in the proposed VCO is analyzed theoretically and verified experimentally. It is demonstrated that with strong coupling among the triple-coupled LC tanks, the proposed VCO achieves a good FOM with an optimized trade-off among wide tuning range, low phase noise, high output power and PAE simultaneously.

Acknowledgment

The authors are thankful to Tower Jazz Semiconductors for their support on the fabrication.

References

[1] C.-K. Hsieh, K.-Y. Kao, J. R. Tseng, and K.-Y. Lin, "A *K*-band CMOS low power modified Colpitts VCO using transformer feedback," in *IEEE MTT-S Int. Microw. Symp. Dig.*, Jun. 2009, pp 1293-1296.

[2] H.-Y. Chang, and Y.-T. Chiu, "*K* -Band CMOS Differential and Quadrature Voltage-Controlled Oscillators for Low Phase-Noise and Low-Power Applications," *IEEE Trans. Microw. Theory Tech.*, vol. 60, no. 1, pp 46-59, Jan. 2012.

[3] Z.-D. Huang, and C.-Y. Wu, "The Design of double-positive-feedback voltage-controlled oscillator," *IEEE Microw. Wireless Compon. Lett.*, vol. 21, no. 7, pp 386-388, Jul. 2011.

[4] J. Yang, C.-Y. Kim, D.-W. Kim, and S. Hong, "Design of a 24-GHz CMOS VCO with an asymmetric-width transformer," *IEEE Trans. Circuits Syst.II, Exp. Briefs*, vol. 57, no. 3, pp. 173–177, Mar. 2010.

[5] C.-A. Lin, J.-L. Kuo, K.-Y. Lin, and H. Wang, "A 24 GHz Low power VCO with transformer feedback," in *IEEE RFIC Symp. Dig.*, Jun. 2009, pp 75-78.

[6] C.-Y. Kim, J. Yang, D.-W. Kim, and S.Hong, "A K-band quadrature VCO based on asymmetric coupled transmission lines," in *IEEE MTT-S Int. Microw. Symp. Dig.*, Jun. 2008, pp 363-366.

[7] V. Kakani, Y. Jin, and F. F. Dai, "A 25 GHz wide-tuning VCO RFIC implemented in 0.13 um SiGe BiCMOS technology," in *IEEE Bipolar/BiCMOS Cir. and Tech. Meet.*, 2010, pp 5-8.

[8] Y.-J Chen, W.-M Kuo, Z.Jin, J.S. Lee, Y.V. Tretiakov, J.D. Cressler, J. Laskar, and G.G.Freeman, "A low-power ka-band Voltage-controlled oscillator implemented in 200-GHz SiGe HBT technology," *IEEE Trans. Microw. Theory Tech.*, vol. 53, no. 5, pp 1672-1681, May 2005.

[9] V. Jain, B. Javid, and P. Heydari, "A BiCMOS dual-band millimeter-wave frequency synthesizer for automotive radars," *IEEE J. Solid-State Circuits*, vol. 44, no. 8, pp 2100-2113, Aug. 2009.

[10] T.-P. Wang, "A CMOS Colpitts VCO Using Negative-Conductance Boosted Technology," *IEEE Trans. Circuits Syst. I, Reg. papers*, vol. 58, no. 11, pp. 2623–2635, Nov. 2011.

[11] N. Mahalingam, K. Ma, K. S. Yeo, S. X. Mou, and T. B. Kumar, "A low power wide tuning range low phase noise VCO using coupled LC tanks" in *Semi. Conf. Dresden*, Sep. 2011, pp 1-4.

[12] R. Aparicio, and A. Hajimiri , "A noise-shifting differential Colpitts VCO," *IEEE J. Solid-State Circuits*, vol. 37, no. 12, pp 1728-1736, Dec. 2002

[13] J.-C. Nallatamby and M. Prigent, "Phase noise in oscillators – Leeson formula revisted," *IEEE Trans. Microw. Theory Tech.*, vol. 51, no. 4, pp 1386-1394, Apr. 2003.

TABLE I
PERFORMANCE SUMMARY AND COMPARISON OF VCO PERFORMANCE WITH STATE-OF-ART VCOS

Ref.	f_{osc} (GHz)	$L\{f_{@100\ kHz}\}$ (dBc/Hz)	$L\{f_{@1MHz}\}$ (dBc/Hz)	K_{VCO} (MHz/V)	P_{DC} (mW)	FTR (%)	P_{out} (dBm)	PAE (%) (P_{out}/P_{DC})	FOM[1] (dBc/Hz)	Area (mm^2)	Technology
This Work	**22.5 – 26.23**	**-75**	**-107.7**	**550**	**8.2**	**15.309**	**-3.1**	**5.972**	**-186.896**	**0.465 × 0.6#**	**0.18 µm SiGe**
[2]	20.3 – 21.3	-65	-116.4	900	3	4.808	-16	0.837	-175.229	0.6 × 0.6	90nm CMOS
[3]	22 – 23.60	-	-115	1600	1.4	7.018	-23	0.357	-174.621	0.731 × 0.645	0.13 µm CMOS
[4]	24	-62	-100.3	-	7.8	2.2	-13.2	0.620	-152.789	0.7 × 0.6	0.18 µm CMOS
[5]	22.1 – 24.3	-95	-113	1300	3	9.483	-13	1.670	-182.077	0.6 × 0.6	0.13 µm CMOS
[6]	22.07 – 22.90	-90	-121.2	100	187.5	3.691	6	2.123	-182.822	1.1 × 1.4	InGap/GaAs
[7]	23.8-26.3	-73	-85	1650	22	9.980	-	-	-	0.56 × 0.205#	0.13 µm SiGe
[8]	32.4 – 33.1	-75	-99	550	2.64	2.137	-12	2.389	-159.686	0.730 × 0.65	0.12 µm SiGe
[9]	23.68-27.0	-80	-99	1200	10	13.102	-	-	-	-	0.18 µm SiGe
[10]	29.61-30.02	-	-104.1	410	2.3	1.375	-14	1.731	-158.738	0.38 × 0.63#	0.18 µm CMOS

$$FOM_{FTR} = L(fo,\Delta f) - 20\log\left(\frac{f_o}{\Delta f}\cdot\frac{FTR}{10}\right) + 10\log\left(\frac{P_{DC}}{1mW}\right), FOM = FOM_{FTR} - 10\log\left(\frac{P_{out}}{1mW}\right),$$ # - Core Area

[1]FOM is calculated with phase noise at 1 MHz offset